POLITECNICO DI TORINO
Repository ISTITUZIONALE

Aerodynamic Optimization of Quadrotor Blades Operating in the Martian Atmosphere

*Original*
Aerodynamic Optimization of Quadrotor Blades Operating in the Martian Atmosphere / CARRENO RUIZ, M., D'Ambrosio, D.. - (2022). (AIAA SCITECH 2022 FORUM San Diego, CA, USA and online 3-7 gennaio 2022) [10.2514/6.2022-0743].

*Availability:*
This version is available at: 11583/2970270 since: 2022-07-29T07:38:44Z

*Publisher:*
AIAA

*Published*
DOI:10.2514/6.2022-0743

*Terms of use:*

This article is made available under terms and conditions as specified in the corresponding bibliographic description in the repository

*Publisher copyright*
AIAA preprint/submitted version e/o postprint/Author's Accepted Manuscript

(Article begins on next page)

06 September 2026

# Aerodynamic Optimization of Quadrotor Blades Operating in the Martian Atmosphere

M. Carreño Ruiz * and D. D'Ambrosio †
*Department of Mechanical and Aerospace Engineering, Politecnico di Torino, Torino, 10124, Italy*

**The design of Unmanned Aerial Systems (UAS) for Martian flight is a relevant and timely topic. The successful flight of the Ingenuity helicopter recently proved its applicability. We present a numerical approach to the aerodynamic optimization of blades for rotors working in flow regimes with Reynolds number smaller than 15,000. Considering gas density and viscosity, rotation speed, and rotor diameter, most of the rotary-wing falls in the so-called ultra-low Reynolds number regime ($10^3$<Re<$10^4$), while the tip region is in the lower range of the very-low Reynolds number regime ($10^4$<Re<$10^5$), where separation-induced laminar-turbulent transition may occur. Such conditions characterize rotor blades of UAS operating in the Mars' atmosphere or at very high altitudes (30 km) in the Earth's atmosphere. The blade design procedure consists of a two-steps optimization process that includes an initial two-dimensional airfoil design analysis followed by three-dimensional simulations to achieve the chord and twist radial distributions necessary to define the blade geometry.**

## I. Nomenclature

| | | |
|---|---|---|
| $C_Q = \frac{Q}{\rho\pi\Omega^2R^5}$ | = | rotor torque coefficient |
| $C_T = \frac{T}{\rho\pi\Omega^2R^4}$ | = | rotor thrust coefficient |
| $C_P = \frac{P}{\rho\pi\Omega^3R^5}$ | = | rotor power coefficient |
| $C_l = \frac{l}{\frac{1}{2}\rho V^2 c}$ | = | airfoil lift coefficient |
| $C_d = \frac{d}{\frac{1}{2}\rho V^2 c}$ | = | airfoil drag coefficient |
| $c$ | = | airfoil chord |
| $V$ | = | freestream velocity |
| $l$ | = | airfoil lift |
| $d$ | = | airfoil drag |
| $\Omega$ | = | rotation rate in radians per second |
| $RPM$ | = | rotation rate in revolutions per minute |
| $R$ | = | rotor radius |
| $Re$ | = | Reynolds number based on the chord |
| $AOA$ | = | angle of attack |
| $M$ | = | rotor tip Mach number |
| $T$ | = | rotor thrust |
| $Q$ | = | rotor torque |
| $P$ | = | rotor power |
| $\rho$ | = | air density |
| $\gamma$ | = | intermittency |
| $k$ | = | turbulent kinetic energy |
| $Re_\theta$ | = | momentum thickness Reynolds number |
| $\omega$ | = | specific dissipation rate |

*PhD Student, Department of Mechanical and Aerospace Engineering, Politecnico di Torino, C.so Duca degli Abruzzi, 24, 10124 Torino, Italy, manuel.carreno@polito.it

†Adjunct Professor, Department of Mechanical and Aerospace Engineering, Politecnico di Torino, C.so Duca degli Abruzzi, 24, 10124 Torino, Italy, domenic.dambrosio@polito.it

## II. Introduction

FLYING in the Mars atmosphere is challenging because the low density characterizing the atmosphere requires a specific aerodynamic design. In fact, despite Mars's gravity being about 38% of Earth's gravity, density is two orders of magnitude smaller than on Earth, which limits the capability of conventional propellers/wings to provide sufficient thrust/lift. Increasing the speed of aerodynamic surfaces to counteract the low-density effect on aerodynamic forces is constrained by the fact that the speed of sound on Mars is about 75% of the speed of sound on Earth at sea level so that the velocity needed to reach critical Mach numbers is lower on Mars than on Earth. In addition, high speed will also increase drag, which may require additional weight for powerful motors and may lead to motor heating issues also.

For the 2D analysis, we performed compressible Navier-Stokes simulations using an unsteady laminar solver. We included compressibility effects because low-temperature conditions and (for Mars) the small gas constant give a smaller-than-usual speed of sound, which, added to the high rotation speed needed to produce thrust in a low-density environment, results in a high subsonic Mach number. For these simulations, we used the commercial Computational Fluid Dynamics (CFD) code STAR-CCM+, and we employed its embedded Adjoint Navier-Stokes method to obtain optimal geometries for appropriate values of Mach and Reynolds numbers. We finally compared our optimized airfoils with other efficient geometries proposed in the literature [1–3] for similar operating conditions.

To design the three-dimensional blade geometry, we used two tools with different fidelity levels, starting from the simplest Blade Element Momentum Method (BEM) and ending with a complete Navier-Stokes simulation of the blades. We selected the best performing geometries using an Evolutionary Algorithm (EA) to avoids local optimums, which occur in a rotor performance optimization process due to the close coupling between design and operation variables. Using low-fidelity simulation tools is necessary as the computational cost of performing an optimization strategy with full Navier-Stokes CFD simulations is computationally very expensive.

Since the optimal twist distribution provided by reduced order models might be considerably different [1, 4] from the results of a Navier-Stokes optimization, we used a three-dimensional Adjoint Navier-Stokes optimization method to produce a further performance improvement taking into account three-dimensional effects that only CFD simulations can capture. The large solidities required to obtain sufficient thrust in such low-density conditions and the three-dimensional flow that this would imply makes it unclear whether low fidelity tools based on lifting line theory can capture optimal rotor chord distribution. For this reason, we repeated the Navier-Stokes-based optimization process for several chord distributions to verify the influence of rotor chord distribution on optimal blade performance. These chord distributions were obtained through a BEM optimization penalizing the mass of the blades.

## III. Airfoil optimization

We proceeded with an initial optimization exercise using the adjoint solver included in STAR-CCM+[5]. Starting from a flat plate with 2% thickness and rounded edges, we obtained a profile that optimizes the aerodynamic efficiency or lift-to-drag ratio. We performed the optimization for Re=3000 and Mach=0.5. In Fig. 3, we compare the resulting airfoil shape with the clf5605 airfoil used at 0.75 of the span for the JPL's Mars Helicopter Ingenuity [2, 6], with an airfoil proposed for a Martian drone in [1] and with the NACA-6904 airfoil (6% camber at 90% chord and 4% thickness) selected in [3] as a reference for Martian conditions.

As the adjoint solver is not directly compatible with unsteady flow conditions, we performed these initial optimization runs using a steady-state solver. For low angles of attack, before the leading edge vortex forms, the solution found by the steady solvers appears to be consistent with the unsteady solver, except for the wake region, where the steady-state solver predicts an attached vortex and the unsteady solver predicts the shedding of vortices. There are some cases, such as, for example, the initial flat plate geometry, in which the steady solver is not able to produce a steady-state solution, but artificial 'periodical' oscillations persist. Fortunately, 'efficient' airfoils are more prone to a steady-state solution. Possibly, this is due to the attached flow in most of the suction-side of the airfoil, where unsteadiness is only present in the trailing edge due to vortex shedding. Vortex shedding produces a net increase in the efficiency of the airfoil. We did not use the unsteady solver after every steady adjoint iteration, but only at the end to check the actual improvement of the optimization process to save computational time. The optimized airfoil that we obtained has a very flat suction side, and it concentrates the camber at the leading and trailing edges. The maximum camber is about 5.2%, very close to the trailing edge, and it shares some similarity with the NACA-6904 proposed in [3]. The average thickness is around 2%. A lower relative thickness could increase the efficiency, but we decided to stop the optimization process when the overall thickness falls below this value. We show the aerodynamic characteristics of the airfoil and a comparison with those of the initial flat plate in Table 1.

The airfoil is optimal for M=0.5, Re=3000, and AOA=6º, but not necessarily for the rest of the polar and other

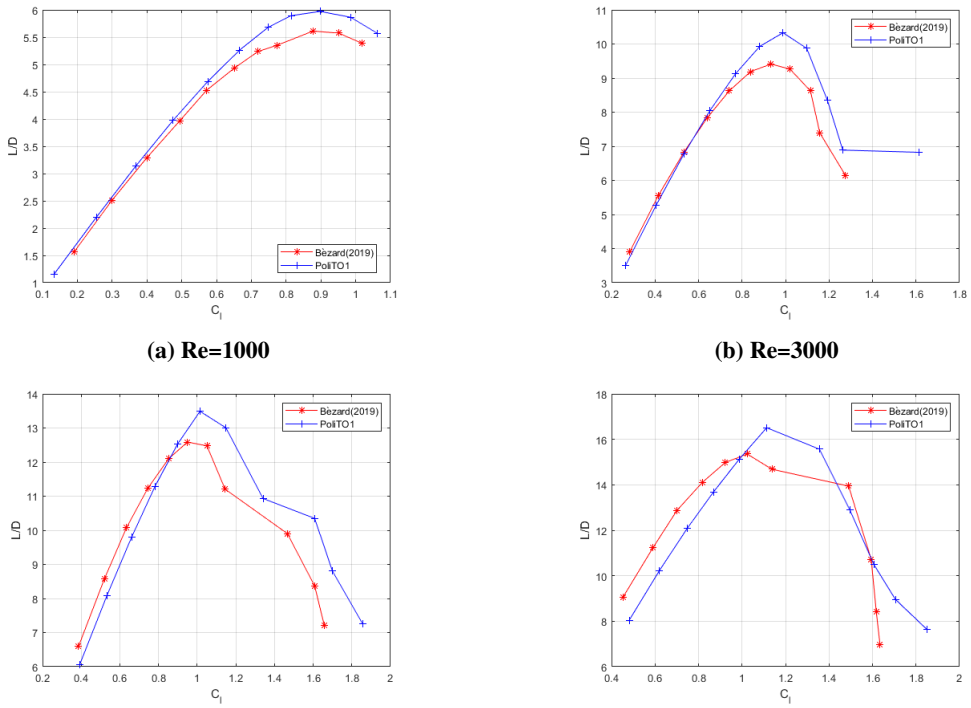


**(a) Re=1000** **(b) Re=3000**

**(c) Re=6000** **(d) Re=10000**

**Fig. 1 Comparison of aerodynamic efficiency between PoliTO1 and Bèzard(2019)[1] at different Reynolds numbers.**

conditions. However, comparing its performances with those declared by other authors for an optimized airfoil for similar conditions [1], the result appear to be promising, as shown in Table 2 and Figure 1. It is clear how the adjoint optimized airfoil achieves the best improvement for Reynolds numbers close to 3000, while for Re = 10000, its performance starts to degrade, possibly due to its aggressive shape. An alternative to avoid this degradation is to perform a multiple-conditions adjoint optimization for different Reynolds numbers or even generate different airfoils for different radial stations as the optimal camber decreases as the Reynolds number is increased [4]. In this case, as the whole geometry will be modified in the 3D adjoint optimization, this airfoil is just a first approximation to a good performing geometry which then will be further optimized. The polar of this airfoil was computed for angles of attack from 0 to 10 degrees and for 8 different Reynolds numbers comprised between 1,000 and 15,000. To avoid an excessive computational cost, the Mach number was left constant at a value of 0.5. This value of the Mach number is close to the tip Mach number for the considered rotation rates. [1] shows a small dependency of airfoil performance with Mach number ranging from 0.1 to 0.5 compared to the effect of the Reynolds number variation and therefore it is considered that a polar calculated at a constant Mach number would generate sufficiently satisfactory results when used by the BEM method, especially considering that the final refinement of the blade in the 3D adjoint optimization will take into account compressibility effects.

**Table 1 Aerodynamic characteristic of the optimized airfoil for M=0.5, Re=3000, AOA=6°.**

| Adjoint Iteration | Cl (Mean value) | Cd (Mean value) | L/D (Mean value) |
|---|---|---|---|
| 1(Flat plate) | 0.49 | 0.083 | 5.9 |
| 50(PoliTO1) | 0.977 | 0.095 | 10.3 |

**Table 2 Comparison between optimized airfoils at M=0.5, Re=3000, AOA=6°.**

| PoliTO1: L/D 6deg | Bezard et al. [1]: L/D 6deg | Δ L/D (%) |
|---|---|---|
| 10.3 | 9.3 | 10.8 |

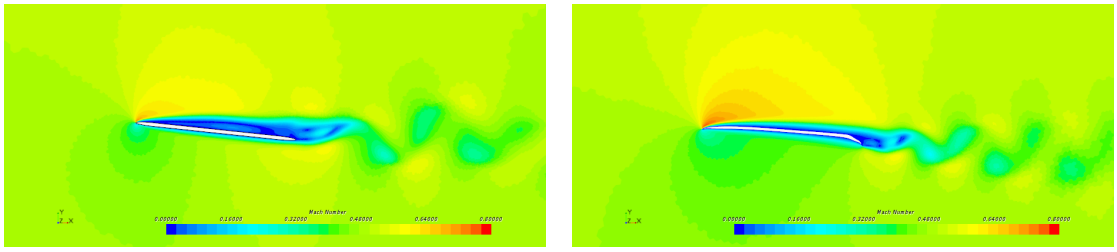

**(a) Initial airfoil(Flat plate).** **(b) Final airfoil(PoliTO1)**

**Fig. 2 Instantaneous velocity field around a at an angle of attack of 6º, Re=3000 and M=0.5.**

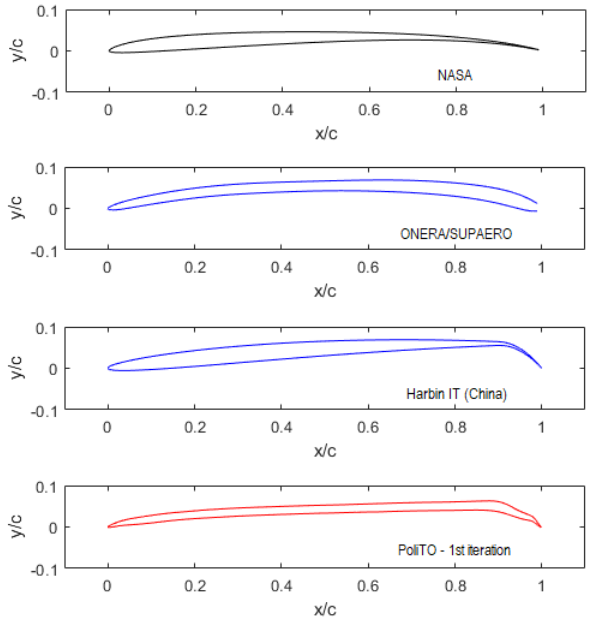


**Fig. 3 Different airfoil geometries reported in literature.**

## IV. Blade optimization

### A. BEM optimization

We performed an initial optimization using an in-house BEM solver implemented in MATLAB. Details about its development and validation can be found in [7], and [8, 9], respectively. We also included a classical angular momentum viscous swirl correction as its effects might be important in the ultra low Reynolds number regime as suggested in [4].

We parametrized both chord and twist distributions using 4 degrees of freedom and spline interpolation along the radial coordinate. The rotor diameter is fixed at 0.4 m, while the rotation rate is considered a design parameter.

The objective function in our optimization is the power loading, T/P. It represents the minimal power for a given thrust, which is appropriate to define the performance of a Martian UAS. We also included a quadratic penalization function to avoid the thrust dropping below a required value, namely 1.1 N in our case. This thrust value will allow to lift a mass of 300g in Mars and therefore the mass budget for the complete quadcopter would rise to 1.2kg.

Initially, we adopted an Evolutionary Algorithm (EA) with considerable population size and a small number of generations (approaching a Montecarlo simulation). In this way, we obtained different geometries, though well-performing, as shown in figure 4 and table 3. Each of these geometries was optimized using a gradient-based approach to find distinct local optima. The performance of these blades is almost identical (<1%), even though the geometries are considerably different. This outcome suggests that our design space is full of local optima and, more precisely, that each chord distribution has an associated pitch distribution that performs almost as well as the global optimum. This is conceptually similar to a variable pitch propeller which show a very small dependency of the maximum propulsive efficiency with the flight velocity as shown in [10]. Furthermore, the twist distribution reveals that all blades work at angles of attack, which are slightly higher than the optimal angle of attack that maximizes aerodynamic efficiency at every station. It also seems clear that the design should base the choice of the chord distribution also on different criteria, such as three-dimensional aerodynamic effects or structural considerations.

**B. Navier-Stokes evaluations of BEM optimal Blades**

To assess the results obtained with the 2D code, we performed Navier-Stokes simulations of the blades with a twofold aim. First, to verify the capability of the BEM code to predict the twist distribution, and second to understand the influence of different geometries in the three-dimensional aerodynamics around the rotating blades. All the CFD calculations presented here are in the laminar regime, though there might be some separation-induced transition on those blade sections at the highest Reynolds number. The maximum Reynolds number for blade OPT1 at its specified rotational speed is 15000 at a radial position of 16 cm. In these conditions, the $\gamma$-$\mathrm{Re}_\theta$ transition model [11] was used to check whether boundary layer transition might be present or not. We found low values of wall intermittency for the whole blade, indicating that the flow remains laminar at these combinations of Reynolds numbers and angles of attack. Figure 5 shows the typical intermittency distribution in laminar flows, with values very close to zero inside the boundary layer and one outside. Transition models are indeed highly empirical, and they may miss transition to turbulence due to flow complexity and the fact that their design is not optimized for these Reynolds numbers. In any case, we believe that most of the blade will remain laminar, and in this paper, we will work under the assumption that Navier-Stokes equations are a reliable mathematical model to predict rotors' performance in Mars atmosphere, as shown in [1].

The laminar solver in STARCCM+ has been validated by the authors in [12] comparing CFD simulations with the experimental results presented by [13] where an ultra low Reynolds numbers flow around a triangular airfoil wing is reproduced inside the Martian Wind Tunnel(MWT) at Tohoku University. The grids for the calculations of the rotors presented in these paper are around 12 million cells and a sliding grid approach has been used with a second order temporal scheme with a time step equivalent to 0.5º of angular displacement of the blade and 10 rotor revolutions are simulated which is enough for thrust and torque convergence.

**Table 3 Optimal geometries BEM and CFD performance.**

| Blade-Solver | Thrust(N) | Torque(N) | T/P (N/W) |
|---|---|---|---|
| OPT1-BEM | 1.10 | 0.0446 | 0.0405 |
| OPT1-CFD | 0.995 | 0.0480 | 0.0341 |
| OPT2-BEM | 1.10 | 0.0451 | 0.0401 |
| OPT2-CFD | 1.00 | 0.0489 | 0.0336 |
| OPT3-BEM | 1.10 | 0.0466 | 0.0402 |
| OPT3-CFD | 0.988 | 0.0491 | 0.0342 |

Table 3 shows how BEM over-predicts thrust in all cases by approximately 10% and under-predicts torque by 10%, which results in a loss of power loading of about 20%. This trend is compatible with an over prediction of the lift coefficient. The two-dimensional CFD simulations revealed an unsteady vortex shedding that produced a noticeable rise in the lift coefficient. Such an effect is not present in the three-dimensional flow. In any case, we assume that these results are reasonably accurate considering the substantial simplifications incorporated in a two-dimensional lifting-line-based theory such as the BEM method. Comparing CFD and BEM power loading for different geometries, we observed an interesting trend: the values predicted by CFD are 20% smaller than BEM results, but the effect is almost identical for all the blades, which is impressive considering the different rotation rates and chord and twist distributions.

The simplest way to match the thrust constraint would be to increase the rotation rate proportionally with the square

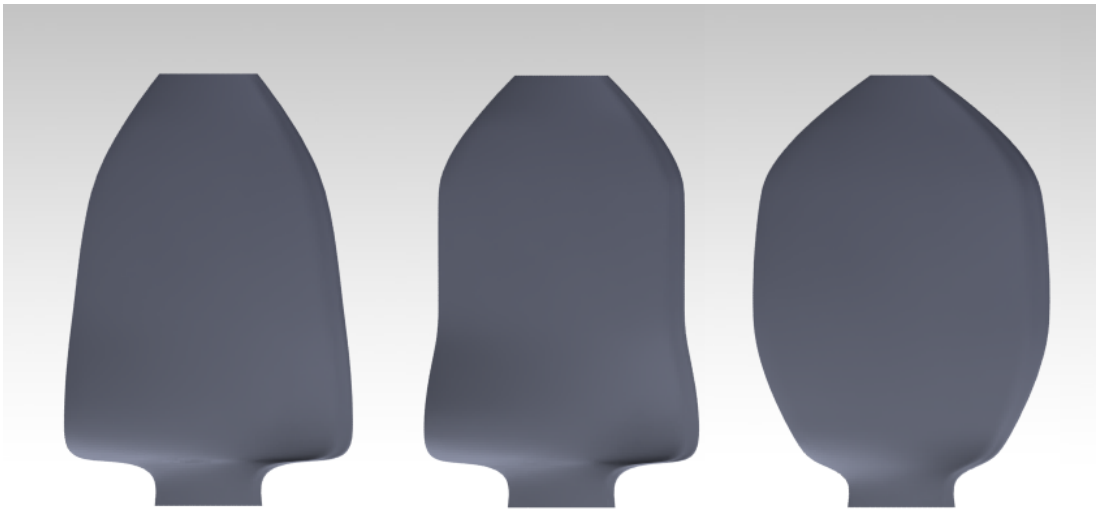

**Fig. 4 BEM optimal blade geometries.From left to right, OPT1, OPT2 and OPT3.**

**Table 4 Effect of increasing rotation rate for OPT1 geometry.**

| | RPM | Thrust(N) | Torque(N) | T/P (N/W) |
|---|---|---|---|---|
| CFD | 5809 | 0.995 | 0.0480 | 0.0341 |
| Theory | 6109 | 1.1 | 0.0531 | 0.0324 |
| CFD | 6109 | 1.103 | 0.0533 | 0.0323 |
| CFD(Iter1) | 6101 | 1.100 | 0.0532 | 0.0324 |

**Table 5 Optimal geometries predicted performance fulfilling thrust requirement.**

| Blade | RPM | Thrust(N) | Torque(N) | Power(W) |
|---|---|---|---|---|
| OPT1 | 6109 | 1.1 | 0.0531 | 33.97 |
| OPT2 | 6091 | 1.1 | 0.0538 | 34.31 |
| OPT3 | 5925 | 1.1 | 0.0547 | 33.94 |

root of the ratio between the desired thrust and the actual thrust. According to dimensional analysis, this relationship only holds for constant Reynolds and Mach numbers, but in our case, the required variation is so slight that Reynolds and Mach don't change significantly, and the relationship holds. We demonstrate this fact in Table 4 for the OPT1 geometry. Table 5 shows the comparison between the blade performances using the theoretical extrapolation. It is worth noting that if the rotational speed rises, the extrapolation is conservative because the actual Reynolds number also increases, leading to an enhancement in performance. Here we used such extrapolation technique to fix the thrust constraint to perform a direct comparison of power consumption. We extrapolated only when thrust was close (less than 10%) to 1.1 N, while we performed an intermediate CFD simulation in case of significant discrepancies. The three blades perform very similarly despite the evident differences in their geometries.

### C. Navier-Stokes Adjoint optimization

We carried out another optimization activity to try to account for the three-dimensional effects that the initial BEM optimization might have neglected. The Adjoint flow solver in STAR-CCM+ is only available for the steady solver, but we showed in [9, 14, 15] that steady-state calculations using a Moving Reference Frame (MRF) approach provide results that are comparable to the unsteady sliding mesh approach. However, the steady solver does not capture the effect of

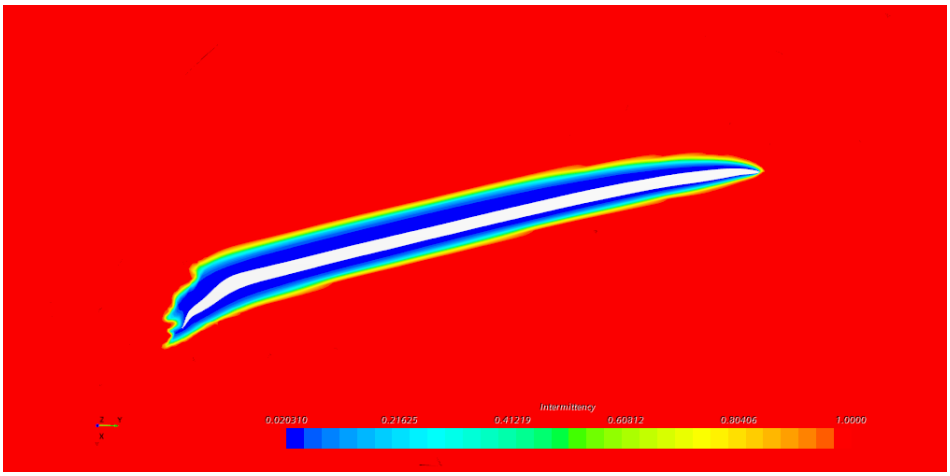


**Fig. 5 Intermittency at a radial station r/R=0.8 for the blade OPT1 at 6109 RPM.**

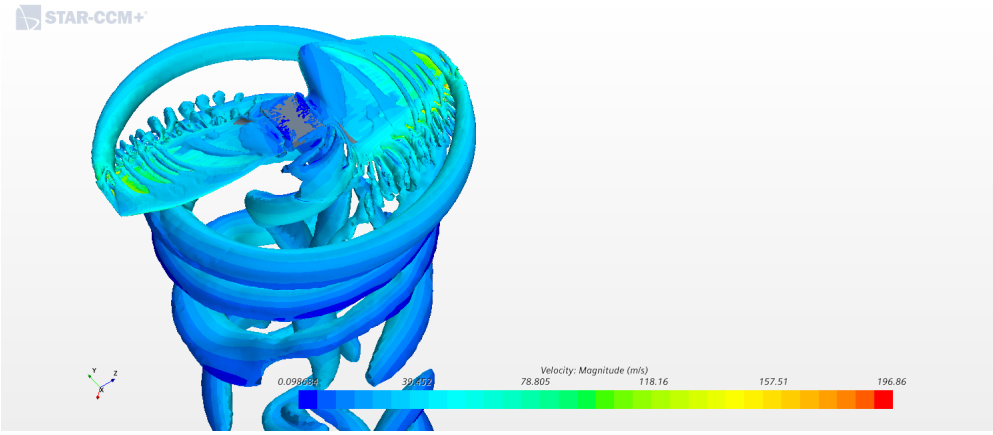


**Fig. 6 Q-criterion iso-surface colored with Velocity magnitude obtained with unsteady solver for blade OPT1.**

vortex emission from the trailing edge seen in the unsteady simulations, which improves the blade performance in a similar way as in the two dimensional simulations. In any case, the overall consistency between steady and unsteady solutions suggests that an optimal shape obtained using steady-state simulations will also improve the performance in time-dependent conditions. Figure 6 shows the flow visualization via the Q-criterion obtained with the unsteady solver. These simulations are performed employing a periodic boundary condition that allows the simulation of only one blade. The grid in this case is around 5 million cells.

To test these hypotheses, we performed an adjoint optimization using the OPT1 blade as the initial geometry. We adopted a simple Steepest Descend Method with a step not larger than 0.5 mm at each adjoint iteration. A lattice of control points was used as a reference for the mesh morphing and gradient calculations with a slight offset(5mm) from the surface, as shown in figure 7. This reduces the irregularities present on the surface of the blades and thus, the chances of generating a bad quality grid after the mesh morphing. Adjoint flow equations are solved using the Restarted GMRES acceleration method, for more details refer to [5]. The choice of the objective function is critical because using the power loading at a constant rotation rate will give efficient geometries that provide a value of thrust below the required. To avoid this issue, we penalized the power loading according to dimensional analysis to ensure that, if the thrust drops, it could potentially be recovered by increasing the rotation rate and yet improve the objective function working always at a constant value of the rotation rate. Off course this approximation assumes constant Reynolds and Mach numbers but the variation of the rotation rate is so small that the effect would be negligible. Table 6 shows the improvement after 10 adjoint iterations for which the optimization process converges. The CFD results presented in table 6 correspond to an unsteady Navier-Stokes evaluation of the final blade obtained after the adjoint optimization process showing that the

improvement shown in the steady solutions reflects also in the unsteady simulations even though the unsteadiness near the trailing edge is not resolved in the optimization process. Figure 8 shows how both the angle of attack and airfoil shape is modified and it is evident how the chord is practically unchanged. Three modifications can be appreciated due to the color change. The twist in the tip region is increased considerably, the camber is slightly increased in the central part of the airfoil and it is not as concentrated in the trailing edge and the twist distribution is reduced for the rest of the blade.

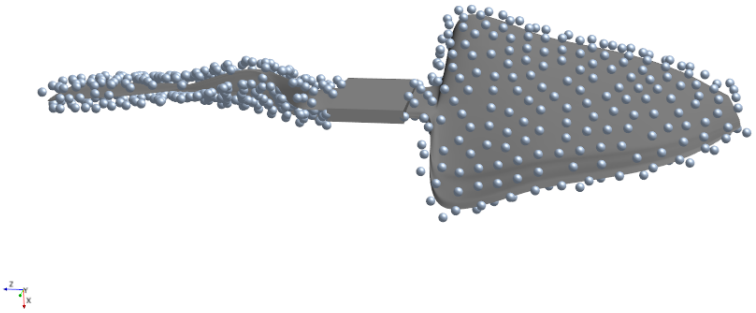

**Fig. 7 Point lattice used for mesh morphing.**

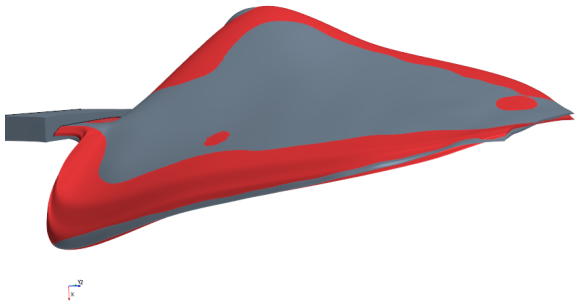

**Fig. 8 Original blade OPT1(red) and adjoint optimized blade OPT1-adj(gray).**

These geometries outperform the blade(Upper-300g) described in [16], which would consume over 43 W(Computed with Free Vortex Wake method[16]) to achieve a thrust level of 1.1 N for a slightly smaller (D=0.3m) three blades rotor in the same density conditions. Such differences raise the question about the importance of size and weight in the Martian context. The blades presented here are aerodynamically efficient, but, considering the low-density conditions on Mars, their weight would be near to the produced thrust, and, thus, their use would be problematic.

**Table 6 Effect of adjoint optimization on blade OPT1**

| Geometry | RPM | Thrust(N) | Moment(Nm) | Power(W) |
|---|---|---|---|---|
| OPT1 | 6101 | 1.1 | 0.0531 | 33.97 |
| OPT1-Adjoint1 | 6212 | 1.1 | 0.0470 | 30.56 |
| Difference(%) | +1.8 | 0 | -11.5 | -10.0 |

### D. Effect of solidity on aerodynamic performance

We repeated the procedure presented above to achieve a compromise solution between aerodynamic optimum and blades weight. In this case, we modified the objective function by subtracting the blade weight on Mars from the generated thrust. We implemented two different corrections. The first one considers a linearly variable thickness, and thus a quadratic penalization, with the chord. The result is an optimal solidity considerably smaller than in the previous geometries. The second correction assumes that the blade has a constant thickness, which could be a realistic approach for some composite manufacturing techniques. In this case, the modification is less aggressive, and the optimal solidity is slightly higher, as shown in Table 7. Figure 9 compares the optimal BEM geometries for the two different corrections. It seems clear that the penalized objective function saves material reducing the chord and increases the pitch and rotation rate to fulfill the thrust requirement. It is also clear that the optimization concentrates mass in the most efficient regions of the blade, reducing the chord length in the inner radial stations compared to the OPT1 geometry. Table 8 shows that the most significant increase in power for a constant thrust is about 2%, which is way smaller than the additional power needed to compensate a large blade mass. With this simplified study, we don't mean to define an optimal rotor, as we didn't consider the structural implications of having thin blades. We wish to emphasize that a careful choice of blade chord distribution should not be based only on aerodynamics but also on mechanical and structural aspects. The importance of weight is critical when densities are as low as on Mars. Another interesting observation from this study is that our optimization procedure generates almost equally performing blades regardless of the chord distribution. It seems that the consumed power to supply an equivalent thrust level decreases with blade solidity, but we have to test more geometries to check if this trend holds for intermediate solidities.

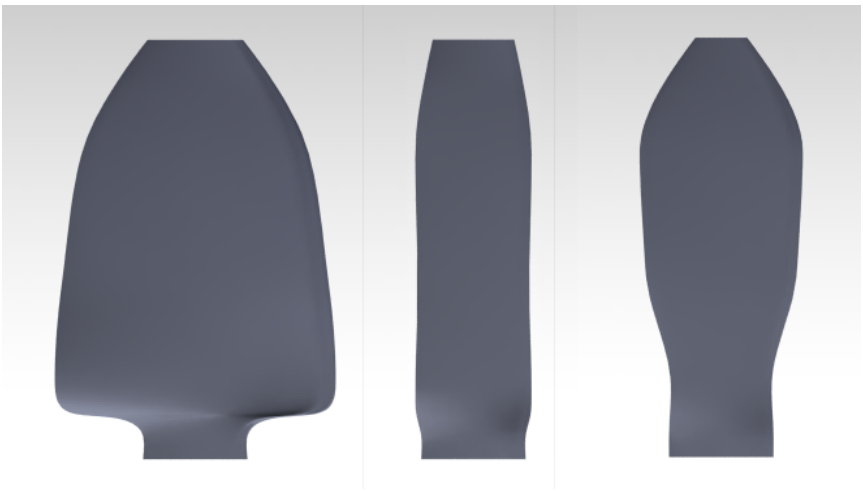

**Fig. 9 BEM optimal blade geometries .From left to right, no mass(OPT1), linear thickness(OPT4) and constant thickness weight penalization(OPT5).**

**Table 7 Geometrical blade characteristics**

| Geometry | solidity | Predicted mass(g) | Weight(N) |
|---|---|---|---|
| OPT1-Adj | 0.297 | 101.6 | 0.378 |
| OPT4-Adj | 0.142 | 21.5 | 0.080 |
| OPT5-Adj | 0.164 | 30.1 | 0.112 |

## V. Conclusions

The multi-fidelity optimization procedure described in this paper provides aerodynamically efficient blades for different solidities and chord distributions. We have also combined global optimization algorithms (Evolutionary Algorithm) with local gradient-based optimization (both in BEM and CFD-Adjoint) to individuate different local

**Table 8 Effect of solidity on consumed power**

| Geometry | RPM | Thrust(N) | Moment(Nm) | Power(W) |
|---|---|---|---|---|
| OPT1-Adj | 6212 | 1.1 | 0.0470 | 30.56 |
| OPT4-Adj | 7465 | 1.1 | 0.0398 | 31.09 |
| OPT5-Adj | 7369 | 1.1 | 0.0398 | 30.71 |

optima in blade performance. The objective function, power loading, seems to have very similar local maximums for noticeably different combinations of geometrical (chord and twist distributions) and operational (rotation rate) design variables. Though the flowfield around 2D airfoils and 3D blades showed some degree of unsteadiness in time-dependent simulations, the adjoint optimization has proven reliable in obtaining well-performing geometries even though it uses the steady Navier-Stokes equations, formulated in a rotating reference frame for the 3D case. The 3D adjoint optimization designed an almost constant chord distribution revealing a preference to modify twist and airfoil distributions. An interesting conclusion that we can draw observing the three adjoint-optimized blades is that even though the CFD evaluations of BEM optimal blades were considerably different from the BEM evaluations, the final Adjoint optimal blade CFD evaluations show very close values to the original BEM evaluations but obtained at a slightly higher rotation rate. The authors believe the adjoint solver twists the blade to compensate the inaccuracies introduced by the BEM estimations of the inflow angles.

## References


[1] Bézard, H., Desert, T., Moschetta, J.-M., and Jardin, T., "Aerodynamic design of a Martian micro air vehicle," *EUCASS 2019*, MADRID, Spain, 2019. URL `https://hal.archives-ouvertes.fr/hal-02397054`.

[2] Koning, W. J., Romander, E. A., and Johnson, W., "Optimization of Low Reynolds Number Airfoils for Martian Rotor Applications Using an Evolutionary Algorithm," *AIAA Scitech 2020 Forum*, 2020, p. 0084.

[3] Zhao, P., Quan, Q., Chen, S., Tang, D., and Deng, Z., "Experimental investigation on hover performance of a single-rotor system for Mars helicopter," *Aerospace Science and Technology*, Vol. 86, 2019, pp. 582–591.

[4] Kunz, P. J., "Aerodynamics and design for ultra-low Reynolds number flight," Ph.D. thesis, Standford University, 2003.

[5] Siemens Digital Industries Software, "Simcenter STAR-CCM+ User Guide v. 2019.3," , Siemens 2019.

[6] Koning, W. J., Johnson, W., and Allan, B. G., "Generation of Mars Helicopter Rotor Model for Comprehensive Analyses," *AHS Aeromechanics Design for Transformative Vertical Flight*, 2018.

[7] Scanavino, M., "Design and testing methodologies for UAVs under extreme environmental conditions," Ph.D. thesis, Politecnico di Torino, 2021.

[8] Carreño Ruiz, M., Manavella, A., and D'Ambrosio, D., "Numerical and experimental validation and comparison of reduced order models for small scale rotor hovering performance prediction," *AIAA 2022 SCITECH*, 2022(Accepted).

[9] Manavella, A., "Low Reynolds number propeller performance validation by CFD analysis and reduced order models," Master's thesis, Politecnico di Torino, 2021.

[10] McCormick, B. W., "Aerodynamics, aeronautics, and flight mechanics," 1995.

[11] Langtry, R. B., and Menter, F. R., "Correlation-based transition modeling for unstructured parallelized computational fluid dynamics codes," *AIAA journal*, Vol. 47, No. 12, 2009, pp. 2894–2906.

[12] Carreño Ruiz, M., and D'Ambrosio, D., "Validation and application of aerodynamic simulations in the Martian atmosphere," *26th Conference of the Italian Association of Aeronautics and Astronautics-AIDAA 2021*, 2021.

[13] Munday, P. M., Taira, K., Suwa, T., Numata, D., and Asai, K., "Nonlinear lift on a triangular airfoil in low-Reynolds-number compressible flow," *Journal of Aircraft*, Vol. 52, No. 3, 2015, pp. 924–931.

[14] Carreño Ruiz, M., Scanavino, M., D'Ambrosio, D., Guglieri, G., and Vilardi, A., "Experimental and numerical analysis of multicopter rotor aerodynamics," *AIAA Aviation 2021 Forum*, 2021.

[15] Carreño Ruiz, M., "CFD simulation of propellers: Best Practices Analysis," Master's thesis, Politecnico di Torino, 2019.

[16] Bézard, H., Désert, T., Jardin, T., and Moschetta, J.-M., "Numerical And Experimental Aerodynamic Investigation Of A Micro-UAV For Flying On Mars," *76th Annual Forum & Technology Display*, 2020.